Graphene actively Q-switched lasers

Diao Li[1,2], Hui Xue[1], Mei Qi[1,2], Yadong Wang[1,3], Sinan Aksimsek[1], Nikolai Chekurov[4], Wonjae Kim[1], Changfeng Li[1], Juha Riikonen[1], Fangwei Ye[5], Qing Dai[6], Zhaoyu Ren[2], Jintao Bai[2], Tawfique Hasan[7], Harri Lipsanen[1] and Zhipei Sun[1]

[1] Department of Electronics and Nanoengineering, Aalto University, Tietotie 3, 02150, Espoo, Finland
[2] State Key Lab Incubation Base of Photoelectric Technology and Functional Materials, and Institute of Photonics and Photon-Technology, Northwest University, 710069 Xi'an, People's Republic of China
[3] MOE Key Laboratory of Space Applied Physics and Chemistry, and Shaanxi Key Laboratory of Optical Information Technology, School of Science, Northwestern Polytechnical University, 710072 Xi'an, People's Republic of China
[4] Oxford Instruments Analytical Oy, Tarvonsalmenkatu 17, 02600, Espoo, Finland
[5] Department of Physics and Astronomy, Shanghai Jiao Tong University, Shanghai 200240, People's Republic of China
[6] National Center for Nanoscience and Technology, 100190 Beijing, People's Republic of China
[7] Cambridge Graphene Centre, University of Cambridge, 9 JJ Thomson Avenue, CB3 0FA, Cambridge, United Kingdom

E-mail: Zhipei.sun@aalto.fi

Keywords: graphene, electro-optic modulators, fiber lasers, active Q-switching

Supplementary material for this article is available online

Abstract

Graphene electro-optic modulators (GEOMs) are emerging as a viable alternative to conventional material-based modulators mainly due to their broadband and ultrafast performance. These GEOMs with combined advantages of small footprint and low energy consumption can potentially enable various high-performance applications that are not possible using conventional approaches. Here, we report the first actively Q-switched lasers with a GEOM. In contrast to the previously reported lasers that are passively modulated by two-dimensional layered material-based saturable absorbers, our actively modulated laser concept represents significant advantages, such as electrically tunable output parameters (e.g. output repetition rate, pulse duration and pulse energy) and electro-optical synchronization. Using a single GEOM, we generate broadband Q-switched pulses at ~1.55 and 2 μm with output energies of up to 123 nJ. This indicates the broadband pulse generation capability of the graphene-based active devices, superior to widely used bulk material-based active modulation approaches. Our results demonstrate a simple and viable design towards broadband, high-repetition-rate, electrically modulated ultrafast lasers for various applications, such as telecommunications and spectroscopy.

1. Introduction

Pulsed lasers have widespread applications in various fields such as spectroscopy, industrial materials processing, and telecommunications [1–4]. Optical pulse generation methods can be generally classified as either active or passive. Active ones normally use externally controlled modulators to actively switch the intra-cavity light, while passive ones typically rely on saturable absorbers (SAs) to introduce self-modulation of the intra-cavity light. Unlike their passively modulated counterparts, actively modulated lasers can enable various laser parameters (e.g. repetition rate, pulse duration and pulse energy) to be electrically tunable [2–4]. This is particularly beneficial to various applications. For example, actively modulated lasers can enable direct synchronization between the generated pulses and an external electrical signal for applications, such as optical transmission, spectroscopy etc, where the optical pulses need to coincide with an electrical signal or temporal positions of the optical pulses from different lasers require temporal coincidence. Further, actively modulated lasers can produce optical pulses with repetition rates much higher than their passively modulated counterparts [2–4]. Bulk electro-optic modulators, such as lithium niobate ($LiNbO_3$) [5, 6], have been widely used for actively modulated lasers [1–4]. However, these bulk optical modulators are typically expensive and complex to fabricate and integrate [5,6], and have severe limitations in performance (e.g. typical operation bandwidth of less than 100 nm [7]). Therefore, novel electro-optic modulators with better performance, cheaper fabrication and easier

integration are of great interest for high performance actively modulated lasers.

Graphene and other two-dimensional (2d) layered materials have shown extraordinary physical properties for various photonic and optoelectronic applications [8–11]. Indeed, numerous devices based on 2d materials have been proposed and demonstrated, such as passive SAs [12–24], electro-optic modulators [25–35], polarizers [36] and photodetectors [37, 38]. Among them, graphene electro-optic modulators (GEOMs) have been demonstrated as a viable alternative to conventional material-based modulators due to their broadband and ultrafast performance, small footprint and low energy consumption [25–35]. Recently, a particularly interesting method is undergoing development to improve the performance of passively modulated lasers with graphene based electro-optic modulators [30–34, 39, 40] (i.e. electrically controlled graphene SAs). For instance, electrically modulated graphene SAs enable different operation regimes (i.e. Q-switching or mode-locking) in fiber lasers [31], and can effectively reduce the self-starting threshold pump power of solid state lasers [32, 33]. However, thus far, graphene actively modulated lasers have not been demonstrated.

Here, we demonstrate broadband pulsed fiber lasers actively modulated with a GEOM for the first time. Unlike the previously reported passively Q-switched lasers with SAs [12, 19, 20], the repetition rate of our pulsed lasers is identical to the frequency of the external electrical modulation signal, and the laser output parameters can be directly adjusted by the electrical signal. This is particularly suitable for various applications, where precise control of the pulse parameters (e.g. relative timing) is needed. Large energy pulse generation at the 1.55 μm telecommunication window (up to 61 nJ) and 2 μm mid-infrared region (up to 123 nJ) was realized with a single GEOM. This demonstrates the wide operation bandwidth of the graphene based active devices for broadband ultrafast pulse generation, superior to traditional bulk material-based active modulation methods.

2. Results and discussion

2.1. Characterization results of the GEOM

A schematic of the GEOM is illustrated in figure 1(a). Double-layer graphene films are separated with an insulating layer of HfO_2 to form a capacitor based modulator configuration [29, 41] (fabrication details in methods). Figure 1(b) shows an optical microscope image of the fabricated device, in which the graphene layers are patterned with a size of 500 × 500 μm^2 (indicated in the white dash square, figure 1(b)). The quality of graphene used in the device is monitored by optical microscopy and Raman spectroscopy before and after each step of the fabrication process. After the device fabrication, the 2D peak of Raman spectrum (figure 1(c)) is still a single sharp Lorentzian with full width at half maximum, FWHM (2D) ~29 cm^{-1}, confirming that monolayer graphene has been successfully transferred. The ratio of D and G peaks (I(D)/I(G)) ≈0.06, showing negligible defects in graphene.

The RC time constant of electro-optic modulators is a key parameter that determines their speed [26, 28, 30]. We measured the RC time constant of our electro-optic modulator with a digital impedance analyzer (HP 4192A). Our experimental results indicate that the modulator has a typical RC time constant of ~2.6 μs (i.e. 3 dB bandwidth of 61.2 kHz). It should be noted that the speed performance of this free-space device is limited compared to the current state of the art of waveguide integrated graphene modulators [25, 26, 30]. We attribute this to the relatively large device footprint (500 × 500 μm^2) and graphene-metal contact resistance (3.25 k$\Omega \cdot \mu$m). Further improvement of the device speed is possible (e.g. optimized device structure and fabrication process [25, 26, 28–33, 35]) for high-repetition-rate actively mode-locked lasers.

When a voltage is applied on the device, an electric field is established by the accumulation of induced carriers at graphene surfaces. Therefore, the broadband absorption in graphene can be effectively controlled by tuning the Fermi energy (E_F) of graphene with electrostatic doping. Interband transitions with energy below 2 × E_F become forbidden due to Pauli blocking [42, 43]. To quantify this light modulation effect, we characterized the optical transmittance of the GEOM device with respect to the electrical voltage at 1550 nm wavelength, as shown in figure 1(d). The measured single-pass optical transmittance increases from 85.51% to 86.77% (corresponding to 1.26% absorption change) when the electrical voltage varies from 0 to 5 V (further increase of applied voltage typically leads to dielectric breakdown). Note that large transmittance loss (13.23%) at 5 V is mainly due to optical loss of the device substrate (i.e. ~8% Fresnel loss of the quartz substrate, ~2% insertion loss of the HfO_2 layer) and absorption of graphene (~3.3% in our double-layer graphene device at 5 V). These transmittance losses can be decreased with different approaches (e.g. anti-reflective coating, low-loss insulation layer coating). Transfer matrix method (TMM) [44] was used to calculate the optical absorption at the same wavelength as a function of the electrical voltage (red curve in figure 1(d), see methods). The transmittance of our GEOM was calculated to be 85.52% at zero voltage. For the maximum electrical voltage of 5 V, the numerical transmittance reaches 86.75%, presenting a total change of 1.23% in the absorption. A relatively low offset between the fitted curve and experimental results (<0.25% difference in transmittance, figure 1(d)) is in a reasonable range considering the inevitable measure deviation in the experiments. We also evaluated the Fermi energy dependence on the electrical voltage with the method in [45]. The calculation shows a Fermi level shift of ~0.17 eV corresponding to the experimental voltage range (i.e. 0–5 V, inset of figure 1(d)). Larger Fermi level shift is possi-

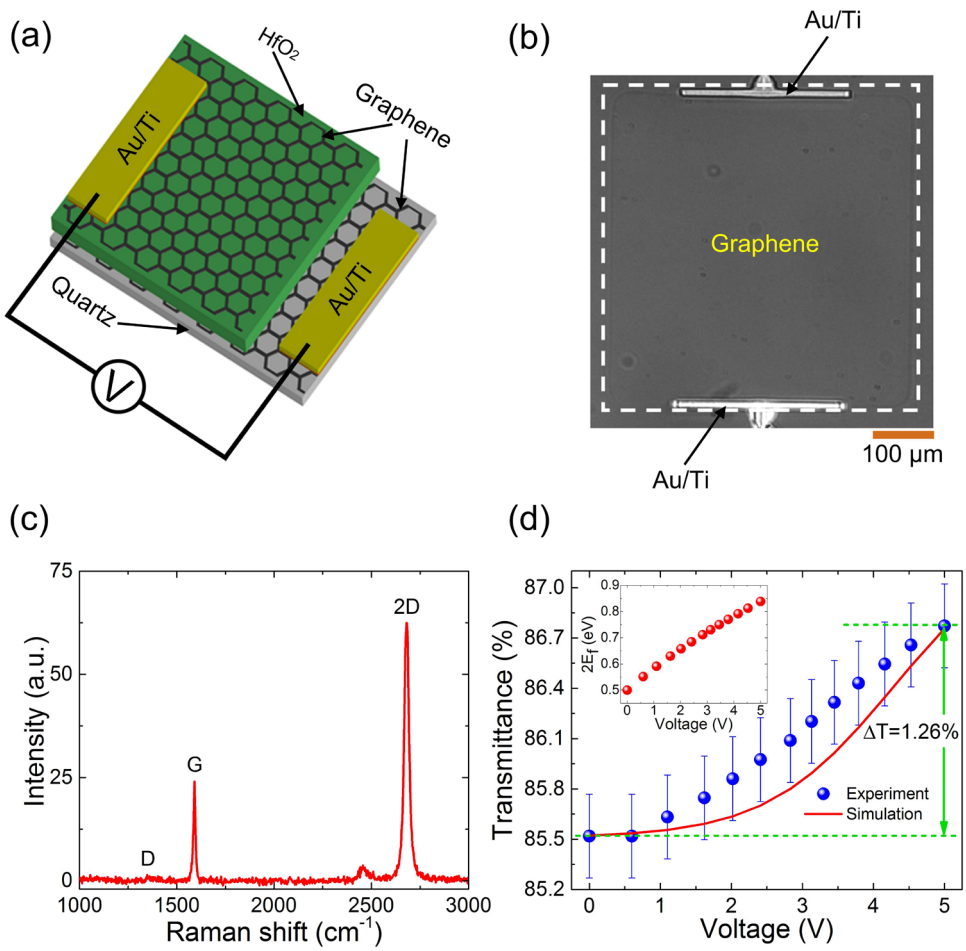

Figure 1. Schematic illustration and characterization of the GEOM device. (a) Three-dimensional sketch and (b) Optical microscopic image of our GEOM device. (c) Raman spectrum of graphene after device fabrication. (d) Optical transmittance as a function of the electrical voltage from experimental results (blue dots) and theoretical calculation (red curve). Inset: Calculated Fermi energy as a function of the electrical voltage.

ble through the optimization of the device fabrication method (e.g. the quality of the deposited dielectric layer, metal contacts, multilayer graphene) [25, 26, 28–35], which is desirable to increase the modulation depth of the GEOM.

2.2. Actively Q-switched fiber laser at 1.55 μm

We first integrated the GEOM with a fiber laser at the 1.55 μm telecommunication band for actively Q-switched pulse generation. The fiber laser with a ring cavity is schematically illustrated in figure 2(a). A segment of 0.7 m Erbium-doped fiber (EDF) was used as the gain fiber. The EDF was pumped by a 980 nm laser diode (LD) via a 980/1550 nm wavelength division multiplexer (WDM). A polarization independent isolator (ISO) was employed to ensure unidirectional light propagation. To integrate the GEOM into the fiber laser resonator, an optical circulator was used to extract the light out from the ring cavity. A collimating lens L1 and a focusing lens L2 were inserted into the beam path, through which the divergent light emission from the fiber pigtail was collimated and focused, respectively. The beam was then incident on the GEOM and reflected back to the fiber laser cavity by a high reflection mirror M (with a reflectivity of >97% in the 1500–2000 nm wavelength range) at the focal point. Accurate alignment of the GEOM position was realized with a high-resolution (<1 μm) crossed linear translation stage. The transmittance of the device (without applied voltage) is constant (~85.5%) when the distance between the graphene device and the reflection mirror M is less than 18 mm. The input beam is blocked by the metal contacts of our graphene device if the distance is increased further. It is worth noting that our double-pass integration method can increase the modulation depth of our GEOM by a factor of two. This will be effective to modulate the intracavity light for active pulse generation. A polarization controller (PC) was used to adjust the birefringence in the laser. A fiber integrated tunable bandpass filter was inserted to tune the output wavelength. A 10% coupler was used for the output. The total length of the laser cavity is ~13 m.

The experimental results of our graphene actively Q-switched fiber laser at 1.55 μm are shown in figures 2(b)–(f). When a square voltage (figure 2(b)) was applied in our GEOM to adjust the periodical cavity loss for active Q-switching, a stable pulse operation was obtained. The amplitude of the square voltage and

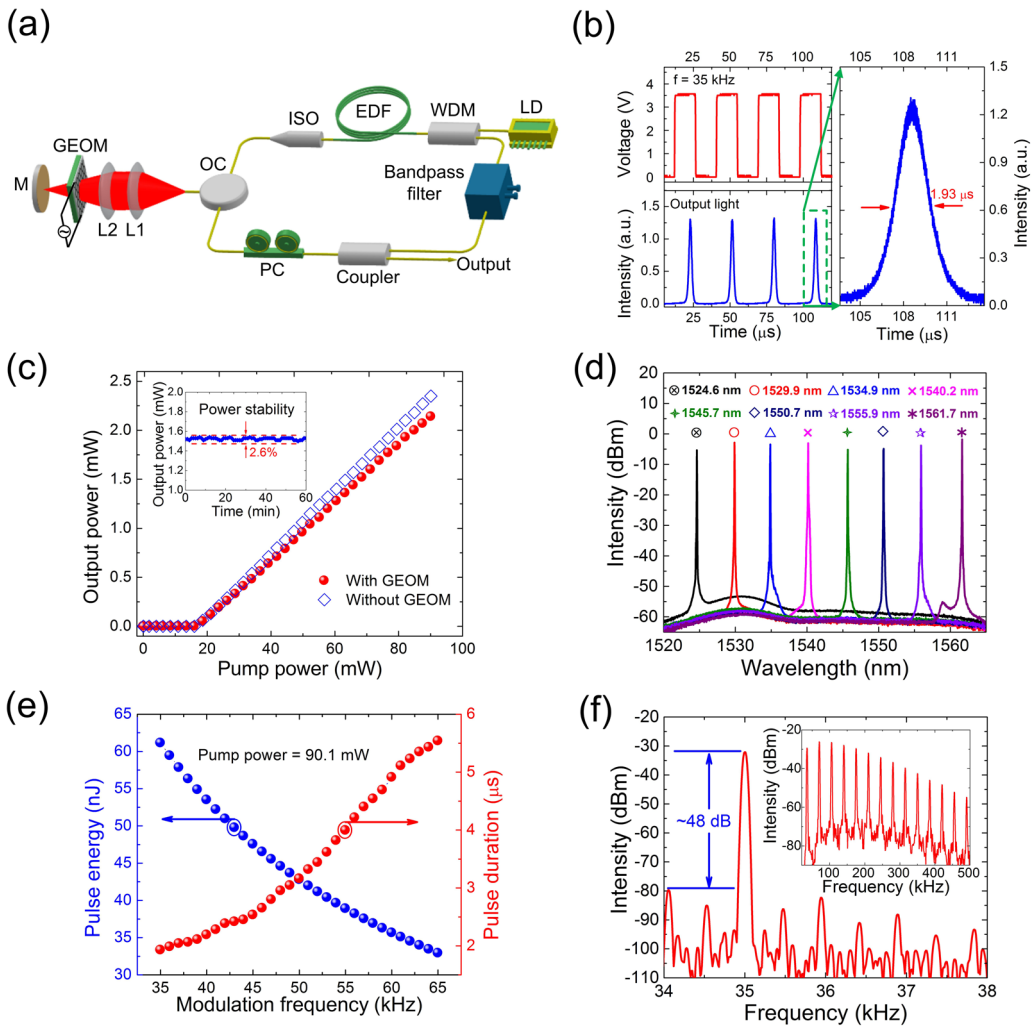

Figure 2. Actively Q-switched fiber laser at 1.55 μm. (a) Laser setup. LD, laser diode; WDM, wavelength division multiplexer; EDF, Erbium-doped fiber; ISO, polarization independent isolator; OC, optical circulator; L1, collimating lens; L2, focusing lens; M, high reflection mirror; PC, polarization controller. (b) Modulation voltage and synchronized output pulse train. Inset, envelop of single pulse. (c) Output power comparison with and without the GEOM. Inset, output power stability of the pulse laser in active Q-switching operation. (d) Wavelength tunable output spectra of the Q-switched laser. (e) Output pulse energy and pulse duration as a function of the modulation frequency. (f) Radio frequency spectrum at the modulation frequency of 35 kHz with a resolution bandwidth of 100 Hz. Inset: 500 kHz wide band radio frequency spectrum with a resolution bandwidth of 1 kHz. Figures (c)–(f) were measured when the output wavelength was 1558.9 nm.

pump power were 3.5 V and 90.1 mW, respectively. Q-switching was not observed in the case without applied voltage. This confirms that our pulse generation is mainly contributed by the active modulation of graphene, i.e. saturable absorption of graphene will not initiate the pulse generation. The optical pulse generation (figure 2(b)) could be interpreted by the operation principle of active Q-switching [2–4]: when the electrical voltage abruptly increases from 0 to 3.5 V, the loss of the GEOM reduces from ~14.5% to 13.2%. This enables cavity feedback and triggers light amplification by stimulated emission in the cavity. Due to a large amount of pump energy stored in the gain medium, the intracavity light intensity builds up rapidly, which results in a short optical pulse with large energy [2–4].

One of the key advantages of actively Q-switched lasers is that the output repetition rate is always identical to the modulation frequency of the electrical signal [2–4], which was clearly observed in our experiment (figure 2(b)). This further confirms that Q-switching is dominated by active modulation of graphene. A close-up image in the inset of figure 2(b) denotes that the typical pulse duration is around 2 μs. The supplementary video also shows the output electrical signal and the output pulses (stacks.iop.org/TDM/4/025095/mmedia). In contrast to the previously demonstrated lasers passively Q-switched with 2d materials [12, 46–48], in which the output repetition rate is determined by various intra-cavity parameters (e.g. gain, loss, cavity length [46–48]), our actively Q-switched laser with repetition rate controlled by external electrical signal is unique. This can facilitate various applications (e.g. telecommunication, spectroscopy and multiple pulse control [1–4]) where pulse synchronization between different pulsed lasers or between optical pulses and electrical signal is critical. It is worth noting that there is a pulse build-up time (i.e. time delay between the rising edge of the electrical signal and the peak of the generated opti-

cal pulses), which can be adjusted by the active modulation parameters (e.g. control voltage and modulation frequency) [49, 50].

The continuous wave emission was observed at a pump power of 18.6 mW, which was changed to Q-switching operation as the applied voltage was increased to 2 V. The pulse train was stablized at 3.5 V. We measured the output average power of our laser in the conditions with and without our GEOM (figure 2(c)). The result shows that the output performance of the laser is slightly affected by the GEOM. For example, the slope efficiency reduced from 3.2% to 3% after inserting the GEOM. The output power of our actively modulated laser is very stable (~2.6% fluctuation, inset of figure 2(c)). The power fluctuation is mainly contributed by the instability of our pump laser diode (~2.5% perturbation in the pump power).

Figure 2(d) depicts the tunable output spectra of the actively Q-switched laser, indicating the broad operation bandwidth of our graphene modulator. The typical FWHM of the output spectra is ~0.05 nm. The output peak wavelength of the Q-switched laser is tunable from 1524.6 to 1561.7 nm by adjusting the intra-cavity bandpass filter. Note that the wavelength tuning range here is mainly limited by the operation bandwidth of the filter, rather than the operation bandwidth of the GEOM, as we also demonstrate active Q-switching at ~2 μm with the same device below.

The output performance (e.g. pulse energy, pulse duration) of our actively modulated laser can be electrically adjusted by the modulation frequency (supplementary video), significantly different from the passively modulated lasers. The measured maximum average output power of the Q-switched laser was 2.14 mW when the pump power reached 90.1 mW, corresponding to the largest output pulse energy of 61 nJ with a repetition rate of 35 kHz. As shown in figure 2(e), the output pulse energy can be adjusted between 61 and 33 nJ (blue dots) in a modulation frequency range from 35 to 65 kHz at the maximum pump power (i.e. 90.1 mW). On the other hand, our modulation frequency change also leads to the variation of the pulse duration, as shown by the red dots in figure 2(e). The pulse duration rises from 1.93 to 5.54 μs when the modulation frequency increases from 35 to 65 kHz. This is because higher repetition rate corresponds to smaller energy stored in the cavity per pulse cycle. Therefore, at higher repetition rate, the stored energy in the cavity releases in a slower speed, generating longer pulses with less pulse energy [2–4].

To investigate the output pulse stability of the Q-switching operation, we measured the radio frequency spectrum of the output pulse train. A signal to noise ratio (SNR) of ~48 dB (corresponding to ~10^5 signal to background contrast) at 35 kHz modulation frequency was achieved (shown in figure 2(f)). We also performed the measurement with a frequency range of up to 500 kHz (inset of figure 2(f)). The spectrum implies an excellent stability of the output pulses [51].

2.3. Actively Q-switched fiber laser at 2 μm

In principle, due to the graphene's broadband operation capability [17, 30, 52], our graphene actively modulated laser concept can be applied for wide band pulse generation. Under this consideration, we subsequently investigated our GEOM for active Q-switching at 2 μm to demonstrate the capability of the optical modulator for longer wavelength. The voltage dependent optical absorption at 2 μm was not measured because of the lack of highly-stable (power variation <1%) light source and detector in the laboratory. Figure 3(a) shows the 2 μm fiber laser setup with a linear cavity. The integration devices (including the collimating lens L1, focusing lens L2, and high reflection mirror M) to couple the GEOM with the light at 1.55 μm (figure 2(a)) were used again for the 2 μm fiber laser. Note that the position of the mirror M (figure 3(a)) needed to be carefully adjusted to reduce the coupling loss due to chromatic aberration of the integration system. A 2 m Thulium/Holmium co-doped fiber (TH512, CorActive) was used as gain medium, which was pumped by a home-made 1570 nm laser through a 1570/2000 nm WDM. A PC was connected to adjust the laser birefringence. A 10/90 fiber coupler at 2 μm was used to extract the light out from the 10% port, and the other ports to form an all-fiber-based reflection mirror.

The actively Q-switched laser performance at 2 μm is shown in figures 3(b)–(f). Figure 3(b) depicts the output pulse train and modulation signal at a frequency of 57 kHz. The amplitude of the square voltage and pump power are 3.1 V and 420 mW, respectively, corresponding to a pulse duration of ~3.5 μs (inset of figure 3(b)). We also observed the synchronization between the output pulse and modulation signal in our pulsed fiber laser at 2 μm. This is a typical fingerprint of active Q-switching, similar to what was observed in our 1.55 μm pulsed fiber laser discussed above.

The active Q-switching starts at 314 mW pump power (figure 3(c)) with a modulation voltage of 3.1 V. This threshold power is considerably high because of the relatively large loss of the intracavity optical components at 2 μm. We measured the average output power of our laser in the cavity configuration with and without the GEOM (figure 3(c)). The result also indicates that the output performance of our 2 μm laser is slightly affected by the GEOM. For example, the slope efficiency reduced by 0.2% (from 6.3% to 6.1%) after inserting the GEOM. The output powers in both cases (with and without GEOM) increase linearly versus the pump power as expected. The measured maximum average output power of the Q-switched laser is 7 mW, with a corresponding pulse energy of 123 nJ at 420 mW pump power. The output power of our 2 μm laser is also very stable (~2.5% fluctuation), comparable with the 1.55 μm fiber laser. During the experiment, no optical damage of the device was observed at this operation power (with a calculated peak power density of ~1.74 mJ cm^{-2}), which identifies the robustness of our GEOM device.

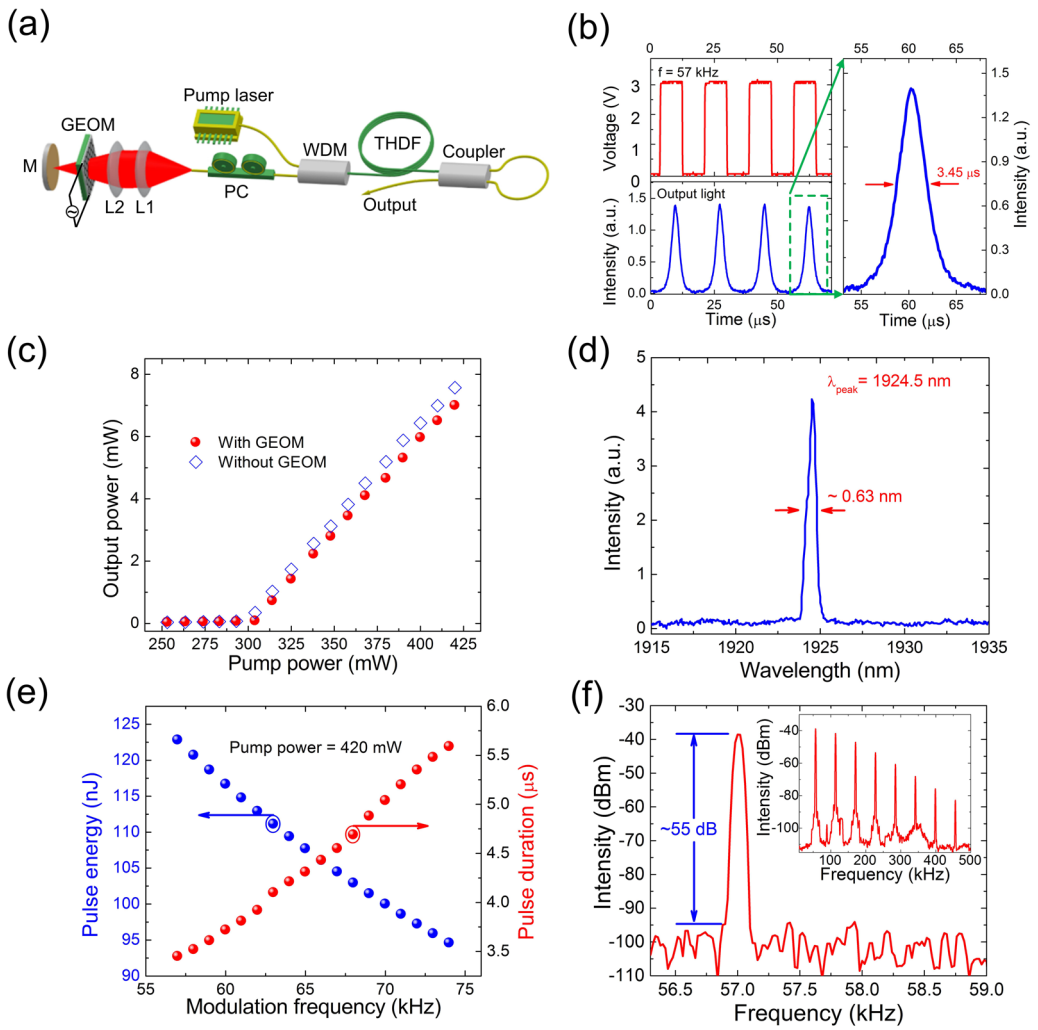

Figure 3. Actively Q-switched fiber laser at 2 μm. (a) Laser setup. THDF, Thulium and Holmium co-doped fiber. (b) Modulation voltage and the synchronized output pulse train. Inset, envelop of single pulse. (c) Output power comparison with and without the GEOM. (d) Q-switched laser output spectrum. (e) Output pulse energy and pulse duration as a function of the modulation frequency. (f) Radio frequency spectrum at the modulation frequency of 57 kHz with a resolution bandwidth of 100 Hz. Inset: 500 kHz wide band radio frequency spectrum with a resolution bandwidth of 1 kHz.

The output spectrum of the Q-switched laser is presented in figure 3(d). The peak wavelength is centered at 1924.5 nm with an FWHM of 0.63 nm. Figure 3(e) shows the pulse energy and pulse duration characteristics as a function of the modulation frequency, when the pump power is fixed to 420 mW (the highest value available in our lab). The pulse energy decreases from 123 to 94.6 nJ (blue dots), and the pulse duration increases from 3.45 to 5.59 μs (red dots), when the modulation frequency rises from 57 to 74 kHz. These electrically tunable behaviors are identical to what we observed with our laser at 1.55 μm.

The output pulse stability of our 2 μm laser was also studied (shown in figure 3(f)). A ~55 dB SNR (corresponding to $>10^5$ signal to background contrast) was measured. We subsequently performed wide band spectrum measurement with a frequency range of up to 500 kHz (inset of figure 3(f)). The spectrum implies highly stable Q-switching operation at 2 μm. We also carried out investigation on long-term (up to 6 months) operation stability of our GEOM and lasers, and did not observe any performance degradation in this time period. Overall, these pulse generation results at 1.55 and 2 μm prove that our GEOM has a broad operation bandwidth (up to >400 nm) for ultrafast pulse generation with a flexibly controlled opto-electronic signal synchronization.

3. Conclusions

In summary, we have demonstrated graphene actively Q-switched lasers. The results show that all key laser parameters can be electrically tunable (e.g. repetition rate, pulse duration, pulse energy). This is completely different from the previously reported lasers that are passively modulated by 2d materials based saturable absorbers. Actively Q-switched pulse train, synchronized with the electrical modulation signal is obtained, with a repetition rate varying from 35 (57) to 65 (74) kHz at 1.55 (2) μm. The wavelength tunability over 37.1 nm bandwidth (from 1524.5 to 1561.7 nm) at 1.55 μm and stable Q-switching at both 1.55 and

2 μm demonstrate the broadband pulse generation capability of the GEOM device. Given by the current state of the art graphene electro-optic modulators (up to 30 GHz [26, 30]), it is expected that an optimized device design with improved performance (e.g. larger modulation speed, higher modulation depth) will enable active mode-locking for ultrafast (<ps) pulse generation with much higher (>GHz) repetition rate. Our results introduce a simple and viable approach towards actively modulated lasers with high repetition rate and broad spectral range for various photonic and optoelectronic applications such as industrial materials processing and spectroscopy.

4. Methods

4.1. Device fabrication and characterization

Monolayer chemical vapor deposition (CVD) grown graphene [53] was transferred to a 1.8×1.8 cm^2 quartz plate ($\sim$210 μm thick) by using the method described in [54]. Bottom contact (titanium/gold, 5/50 nm thickness) to graphene was defined by a conventional Electron Beam Lithography (EBL, Vistec EPBG5000pES) followed by a lift-off process. The graphene sheet was subsequently patterned into a size of 500×500 μm^2 with EBL and reactive ion etching (RIE). Next, atomic layer deposition (ALD, Beneq TFS-500) process was used to directly grow a 30 nm thick HfO_2 on the graphene sheet as a high permittivity dielectric layer [55]. Another CVD grown monolayer graphene was transferred on the dielectric and patterned as its bottom counterpart, in order to form the capacitor based graphene modulator. Metal Ti/Au contact on top was then fabricated by using the same process as described above. The graphene quality in the device is monitored by Raman spectroscopy (Witec alpha 300R, 532 nm excitation) before and after each step in the fabrication process.

4.2. Simulation of voltage dependent graphene absorption

Electrical voltage dependent graphene absorption is typically evaluated with Kubo formula [28, 29, 56] by taking the dielectric and Fermi level of the graphene device into account. The equivalent thickness of graphene monolayers was evaluated [35, 45, 57], and the calculated refractive indexes were normalized according to the experimental value reported by [57] to get realistic results.

4.3. Laser characterization

In order to characterize the actively Q-switched lasers, a high resolution optical spectrum analyzer (Anritsu, MS9740A) was used for the 1.55 μm fiber laser. The output spectrum of the 2 μm fiber laser was measured by an infrared optical spectrum analyzer (WaveScan, APE). An oscilloscope and a frequency spectrum analyzer (Anritsu MS2692A) connected with a broadband ultrafast (>25 GHz) photodetector were used to measure the output pulse train and radio frequency spectrum for both 1.55 and 2 μm.

Acknowledgments

The authors acknowledge funding from the European Union's Seventh Framework Programme (REA grant agreement No. 631610), EU Graphene Flagship (No. 696656), Academy of Finland (No. 276376, 284548, 295777, 304666), China Scholarship Council (CSC), Nokia foundation,the Scientific and Technological Research Council of Turkey (TÜBİTAK), International Science and Technology Cooperation Project (No. 2014DFR10780), the Foundation of the Education Committee of Shaanxi Province (No. 14JK1756, China), the Science Foundation of Northwest University (No. 13NW14), Northwest University Cross-discipline Fund for Postgraduate Students (YZZ13027), and the financial support from Centre for International Mobility (CIMO) under the Finnish Ministry of Education and Culture. ZS and FY acknowledge Funding from the State Key Laboratory of Advanced Optical Communication Systems and Networks, Shanghai Jiao Tong University, China. TH acknowledges funding from RAEng through a research fellowship (Graphex). We also acknowledge the provision of technical facilities of the Micronova, Nanofabrication Centre of Aalto University.

Additional information

This manuscript is accompanied by a supplementary video. The time delay of our graphene capacitor based modulator is not excluded.

Competing financial interests

The authors declare no competing financial interests.

Author contributions

ZS conceived the idea, DL and HX designed the modulator configuration. HX and MQ carried out the device fabrication and measured Raman spectrum. DL and YW performed the laser experiments. SA carried out the theoretical calculation. NC helped to measure the RC time constant. WK, CL and JR prepared the CVD graphene. All authors contributed to the result discussion and manuscript writing.

References

[1] Keller U 2003 Recent developments in compact ultrafast lasers *Nature* **424** 831–38
[2] Fermann M E, Galvanauskas A and Sucha G 2002 *Ultrafast Lasers: Technology and Applications* vol 80 (Boca Raton: CRC Press)
[3] Rulliere C 2005 *Femtosecond Laser Pulses* (New York: Springer)

[4] Paschotta R 2008 *Encyclopedia of Laser Physics and Technology* (New York: Wiley)
[5] Wooten E L *et al* 2000 A review of lithium niobate modulators for fiber-optic communications systems *IEEE J. Sel. Top. Quantum Electron.* **6** 69–82
[6] Wong K K 2002 *Properties of Lithium Niobate* (London: INSPEC)
[7] https://www.thorlabs.com/newgrouppage9.cfm?objectgroup_id=3918
[8] Novoselov K S and Geim A K 2007 The rise of graphene *Nat. Mater.* **6** 183–91
[9] Bonaccorso F, Sun Z, Hasan T and Ferrari A C 2010 Graphene photonics and optoelectronics *Nat. Photon.* **4** 611–22
[10] Ferrari A C *et al* 2015 Science and technology roadmap for graphene, related two-dimensional crystals, and hybrid systems *Nanoscale* **7** 4598–810
[11] Xia F, Wang H, Xiao D, Dubey M and Ramasubramaniam A 2014 Two-dimensional material nanophotonics *Nat. Photon.* **8** 899–907
[12] Martinez A and Sun Z 2013 Nanotube and graphene saturable absorbers for fiber lasers *Nat. Photon.* **7** 842–5
[13] Hasan T, Sun Z, Wang F, Bonaccorso F, Tan P H, Aleksey G R and Ferrari A C 2009 Nanotube-polymer composites for ultrafast photonics *Adv. Mater.* **21** 3874–99
[14] Bao Q, Zhang H, Wang Y, Ni Z H, Yan Y L, Shen Z X, Loh K P and Tang D Y 2009 Atomic-layer graphene as a saturable absorber for ultrafast pulsed lasers *Adv. Funct. Mater.* **19** 3077–83
[15] Yamashita S 2012 A tutorial on nonlinear photonic applications of carbon nanotube and graphene *J. Lightwave Technol.* **30** 427–47
[16] Sun Z, Hasan T, Torrisi F, Popa D, Privitera G, Wang F, Bonaccorso F, Basko D M and Ferrari A C 2010 Graphene mode-locked ultrafast laser *ACS Nano* **4** 803–10
[17] Zheng Z, Zhao C, Lu S, Chen Y, Li Y, Zhang H and Wen S 2012 Microwave and optical saturable absorption in graphene *Opt. Express* **20** 23201–14
[18] Cho W B, Kim J W, Lee H W, Bae S, Hong B H, Choi S Y, Baek I H, Kim K, Yeom D and Rotermund F 2011 High-quality, large-area monolayer graphene for efficient bulk laser mode-locking near 1.25 μm *Opt. Lett.* **36** 4089–91
[19] Woodward R I, Howe R C T, Hu G, Torrisi F, Zhang M, Hasan T and Kelleher E J R 2015 Few-layer MoS_2 saturable absorbers for short-pulse laser technology: current status and future perspectives *Photon. Res.* **3** A30–42
[20] Li D, Jussila H, Karvonen L, Ye G, Lipsanen H, Chen X and Sun Z 2015 Polarization and thickness dependent absorption properties of black phosphorus: new saturable absorber for ultrafast pulse generation *Sci. Rep.* **5** 15899
[21] Tan W D, Su C Y, Knize R J, Xie G Q, Li L J and Tang D Y 2010 Mode locking of ceramic Nd:yttrium aluminum garnet with graphene as a saturable absorber *Appl. Phys. Lett.* **96** 031106
[22] Sobon G, Sotor J and Abramski K M 2012 Passive harmonic mode-locking in Er-doped fiber laser based on graphene saturable absorber with repetition rates scalable to 2.22 GHz *Appl. Phys. Lett.* **100** 161109
[23] Mary R *et al* 2013 1.5 GHz picosecond pulse generation from a monolithic waveguide laser with a graphene-film saturable output coupler *Opt. Express* **21** 7943–50
[24] Zaugg C A *et al* 2013 Ultrafast, widely tuneable vertical-external-cavity surface-emitting laser and mode-locked by a graphene-integrated distributed Bragg reflector *Opt. Express* **21** 31548–59
[25] Liu M, Yin X, Ulin-Avila E, Geng B, Zentgraf T, Ju L, Wang F and Zhang X 2011 A graphene-based broadband optical modulator *Nature* **474** 64–7
[26] Phare C, Lee Y, Cardenas J and Lipson M 2015 Graphene electro-optic modulator with 30 GHz bandwidth *Nat. Photon.* **9** 511–4
[27] Ding Y, Zhu X, Xiao S, Hu H, Frandsen L H, Mortensen N A and Yvind K 2015 Effective electro-optical modulation with high extinction ratio by a graphene-silicon microring resonator *Nano Lett.* **15** 4393–400
[28] Lee C, Suzuki S, Xie W and Schibli T 2012 Broadband graphene electro-optic modulators with sub-wavelength thickness *Opt. Express* **20** 5264–9
[29] Polat E and Kocabas C 2013 Broadband optical modulators based on graphene supercapacitors *Nano Lett.* **13** 5851–7
[30] Sun Z, Martinez A and Wang F 2016 Optical modulators with 2D layered materials *Nat. Photon.* **10** 227–38
[31] Lee E J *et al* 2015 Active control of all-fiber graphene devices with electrical gating *Nat. Commun.* **6** 6851
[32] Baylam I, Cizmeciyan M N, Ozharar S, Polat E O, Kocabas C and Sennaroglu A 2014 Femtosecond pulse generation with voltage-controlled graphene saturable absorber *Opt. Lett.* **39** 5180–3
[33] Baylam I, Balci O, Kakenov N, Kocabas C and Sennaroglu A 2016 Graphene-gold supercapacitor as a voltage-controlled saturable absorber for femtosecond pulse generation *Opt. Lett.* **41** 910–3
[34] Ma L, Tan Y, Akhmadaliev S, Zhou S and Chen F 2016 Electrically tunable Nd:YAG waveguide laser based on graphene *Sci. Rep.* **6** 36785
[35] Hu Y, Pantouvaki M, Campenhout J V, Brems S, Asselberghs I, Huyghebaert C, Absil P and Thourhout D V 2016 Broadband 10 Gb s^{-1} operation of graphene electro-absorption modulator on silicon *Laser Photon. Rev.* **10** 307–16
[36] Bao Q, Zhang H, Wang B, Ni Z, Lim C H Y X, Wang Y, Tang D Y and Loh K P 2011 Broadband graphene polarizer *Nat. Photon.* **5** 411–5
[37] Xia F, Mueller T, Lin Y, Valdes-Garcia A and Avouris P 2009 Ultrafast graphene photodetector *Nat. Nanotechnol.* **4** 839–43
[38] Koppens F H L, Mueller T, Avouris P, Ferrari A C, Vitiello M S and Polini M 2014 Photodetectors based on graphene, other two-dimensional materials and hybrid systems *Nat. Nanotechnol.* **9** 780–93
[39] Kuse N, Jiang J, Lee C C, Schibli T R and Fermann M E 2016 All polarization-maintaining Er fiber-based optical frequency combs with nonlinear amplifying loop mirror *Opt. Express* **24** 3095–102
[40] Lee C C, Mohr C, Bethge J, Suzuki S, Fermann M E, Hartl I and Schibli T R 2012 Frequency comb stabilization with bandwidth beyond the limit of gain lifetime by an intracavity graphene electro-optic modulator *Opt. Lett.* **37** 3084–6
[41] Liu M, Yin X and Zhang X 2012 Double-layer graphene optical modulator *Nano Lett.* **12** 1482–5
[42] Wang F, Zhang Y, Tian C, Girit C, Zettl A, Crommie M and Ron Y 2008 Shen Gate-variable optical transitions in graphene *Science* **320** 206–9
[43] Li Z Q, Henriksen E A, Jiang Z, Hao Z, Martin M C, Kim P, Stormer H L and Basov D N 2008 Dirac charge dynamics in graphene by infrared spectroscopy *Nat. Phys.* **4** 532–5
[44] Hansen W N 1968 Electric fields produced by the propagation of plane coherent electromagnetic radiation in a stratified medium *J. Opt. Soc. Am.* **58** 380–90
[45] Gosciniak J and Tan D T H 2013 Theoretical investigation of graphene-based photonic modulators *Sci. Rep.* **3** 1897
[46] Popa D, Sun Z, Hasan T, Torrisi F, Wang F and Ferrari A C 2011 Graphene Q-switched, tunable fiber laser *Appl. Phys. Lett.* **98** 073106
[47] Luo Z *et al* 2015 Two-dimensional material-based saturable absorbers: towards compact visible-wavelength all-fiber pulsed lasers *Nanoscale* **8** 1066–72
[48] Li D, Castillo A E D R, Jussila H, Ye G, Ren Z, Bai J, Chen X, Lipsanena H, Sun Z and Bonaccorso F 2016 Black phosphorus polycarbonate polymer composite for pulsed fibre lasers *Appl. Mater. Today* **4** 17–23
[49] Koechner W 2013 *Solid-State Laser Engineering* vol 1 (New York: Springer)
[50] Chang Y M, Lee J, Jhon Y M and Lee J H 2011 Active Q-switching in an erbium-doped fiber laser using an ultrafast

silicon-based variable optical attenuator *Opt. Express* **19** 26911–6
[51] Von der Linde D 1986 Characterization of the noise in continuously operating mode-locked lasers *Appl. Phys.* B **39** 201
[52] Fu B, Hua Y, Xiao X, Zhu H, Sun Z and Yang C 2014 Broadband graphene saturable absorber for pulsed fiber lasers at 1, 1.5, and 2 μm *IEEE J. Sel. Top. Quantum Electron.* **20** 411–5
[53] Riikonen J, Kim W, Li C, Svensk O, Arpiainen S, Kainlauri M and Lipsanena H 2013 Photo-thermal chemical vapor deposition of graphene on copper *Carbon* **62** 43–50
[54] Suk J W, Kitt A, Magnuson C W, Hao Y, Ahmed S, An J, Swan A K, Goldberg B B and Ruoff R S 2011 Transfer of CVD-grown monolayer graphene onto arbitrary substrates *ACS Nano* **5** 6916–24
[55] Huang A P, Chu P K and Yang Z C 2010 *Hafnium-Based High-k Gate Dielectrics* (Rijeka: Intech)
[56] Xu C, Jin Y, Yang L, Yang J and Jiang X 2012 Characteristics of electro-refractive modulating based on graphene -oxide-silicon waveguide *Opt. Express* **20** 22398–405
[57] Jussila H, Yang H, Granqvist N and Sun Z 2016 Surface plasmon resonance for characterization of large-area atomic-layer graphene film *Optica* **3** 151–8